Advanced Physical Research
Vol.6, No.3, 2024, pp.182-190
https://doi.org/10.62476/apr63182

IMPACT OF Ca DOPING ON THE STRUCTURAL CHARACTERISTICS OF $La_{1-x}Ca_xFe_{0.5}Mn_{0.5}O_3$

T.A. Tran[1], H.C. Tran[1], S.H. Le[1], N.T. Nghiem[2], L.V. Truong-Son[3,*], D.T. Khan[3], L.K. Abdullayeva[4], R.F. Hashimov[5,6]

[1]Department of Physics, Ho Chi Minh City University of Technology and Education, Ho Chi Minh, Vietnam
[2]Faculty of Electronics, Electrical Engineering and Material Technology, University of Sciences, Hue University, Hue, Vietnam
[3]The University of Da Nang - University of Science and Education, Danang, Vietnam
[4]Azerbaijan Technical University, Baku, Azerbaijan
[5]Institute of Physics, Ministry of Science and Education, Baku, Azerbaijan
[6]Western Caspian University, Baku, Azerbaijan

Abstract. A series of perovskite compounds $La_{1-x}Ca_xFe_{0.5}Mn_{0.5}O_3$ (x = 0, 0.1, 0.2, 0.3, 0.4, 0.5, 0.6, 0.7, 0.8 and 0.9) were synthesized using the conventional ceramic method. The influence of the Ca-doping on the crystal structure of these compounds was studied using was investigated through X-ray diffraction (XRD) and Raman scattering spectroscopy. XRD analysis revealed that all the samples crystallize in an orthorhombic structure with the *Pbnm* space group. The variation in lattice parameters, bond lengths and bond angles created by the difference in valence state and ion size due to the Ca-doping leads to the distortion and tilt of octahedra in the samples.

Keywords: *Double perovskites, distortion, X-ray diffraction, Raman spectroscopy.*

Corresponding Author: *L.V. Truong-Son, The University of Da Nang - University of Science and Education, DaNang, Vietnam, e-mail: lvtson_kl@ued.udn.vn*

Received: *22 July 2024;* ***Accepted:*** *3 September 2024;* ***Published:*** *16 October 2024.*

1. Introduction

Perovskites are a group of fascinating materials with a common molecular formula of ABO_3, where A represents alkali earth or rare earth elements and B represents transition metal elements. Perovskite oxides have been widely studied due to their important physical properties, such as high dielectric constants, magnetism, superconductivity (Lu *et al*., 2019), ferroelectricity, multiferroicity, pyroelectricity (Geng *et al*., 2020; MącZka *et al*., 2011; Romero *et al*., 2015), piezoelectricity and enhanced electrical resistivity (Guo *et al*., 2020; Zhang *et al*., 2020).

Among perovskites, $LaFe_{0.}5Mn_{0.5}O_6$ (LFMO) have been considered potential candidates for technological devices. Reports in the literature have shown that the LFMO perovskite crystallizes in different crystal structures, depending on synthesis methods such as solid-state, sol-gel, combustion, thermal decomposition, co-precipitation and the

How to cite (APA):
Tran, T.A., Tran, H.C., Le, S.H., Nghiem, N.T., Truong-Son, L.V., Khan, D.T., Abdullayeva, L.K. & Hashimov, R.F. (2024). Impact of Ca doping on the structural characteristics of $La_{1-x}Ca_xFe_{0.5}Mn_{0.5}O_3$. *Advanced Physical Research, 6*(3), 182-190 https://doi.org/10.62476/apr63182

Pechini method. The crystal structure of LFMO can be categorized into three structures: monoclinic crystal, triclinic crystal and cubic crystal with space groups P21/n (Dar *et al*., 2023), Pbnm (Palakkal *et al*., 2018), Pnma (Ahmad *et al*., 2021) and Pm-3m (Dutta *et al*., 2019). The magnetic of perovskites LFMO is quite complex (De *et al*., 2005; 2006; De Lima *et al*., 2010; Gilleo, 1957). The polycrystalline sample of LFMO is considered to have cluster-glass properties with large irreversibility in the magnetic field below 260 K (Glazer, 1972; Mitchell, 2002; Woodward, 1997). The coexistence of ferromagnetic and antiferromagnetic phases has been observed in the LFMO polycrystalline sample and they are related to the random distribution of ions in the B-site positions (Dagotto *et al*., 2003).

Recently, co-doping at La sites in the LFMO also attracted lots of interest. Dutta et al. (2019) doped Ba into $La_{1-x}Ba_xFe_{0.5}Mn_{0.5}O_3$ (x = 0.25, 0.33, 0.5) to enhanced the glass magnetic state at lower temperatures. In addition, when Ba is doped into the sample, additional reflection points (110) appear in electron diffraction (ED) to clearly further clarify the arrangement of Fe and Mn in the B site of perovskite (Dutta *et al*., 2019). On the other hand, when adding impurities of other substances into $La_{1-x}A_xFe_{0.5}Mn_{0.5}O_3$ (x = 0, 0.25 and A = Ca, Sr and Pb) by the sol-gel method, the particle size has a significant impact on the magnetism in $LaFe_{0.5}Mn_{0.5}O_3$ due to the growth of surface ferromagnetic clusters at the nanoscale (Hossain *et al*., 2017). In this article, we study the effect of Ca-doping on the structural properties of perovskites $La_{1-x}Ca_xFe_{0.5}Mn_{0.5}O_3$ (LCFMO) (x = 0, 0.1, 0.2, 0.3, 0.4, 0.5, 0.6, 0.7, 0.8 and 0.9) prepared using the conventional ceramic method utilizing X-ray diffraction (XRD) and Raman spectroscopy analysis.

2. Experimental details

LCFMO compounds with x = 0-0.9 were prepared using the solid-state reaction technique from precursors of La_2O_3, $CaCO_3$, Mn_2O_3 and Fe_2O_3. The stoichiometric mixtures of these oxides were first ground for several hours and then heated in air at 1320°C in successive steps for 15, 5 and 15 h. The obtained mixtures were final annealed at 1375°C for 22 h. The samples was reground between the heating periods. The structural parameters of the LCFMO samples were investigated utilizing X-ray direction and Raman scattering spectroscopy measurements.

3. Results and discussion

Structure analysis was conducted using X-ray powder diffraction data. Rietveld refinement of the samples was performed to determine the structural parameters using the FullProf Suite software. Figure 1(a) illustrates the XRD patterns of some representative LCFMO with x = 0, 0.3, 0.6 and 0.9. The refinement shows that all samples exhibit the orthorhombic structure with the space group of Pnma (Figure 1(b)) indexed as 101, 121, 220, 202, 141, 042, 242 and 161 consistent with the previous reported structure of $LaFe_{0.5}Mn_{0.5}O_3$ (Das *et al*., 2023; Martínez-Rodríguez *et al*., 2018). The lattice parameters such as lattice constants and unit-cell volume of the sample, derived from the XRD data are shown in Figure 2. As we can see, doping Ca into the LCFMO leads to a decrease in the lattice constants and therefore, the unit-cell volume. This decrease in the lattice parameters is due to smaller ionic radius of Ca (0.99 Å) compared to the radius of La^{3+} (1.06 Å) (Li *et al*., 2014).

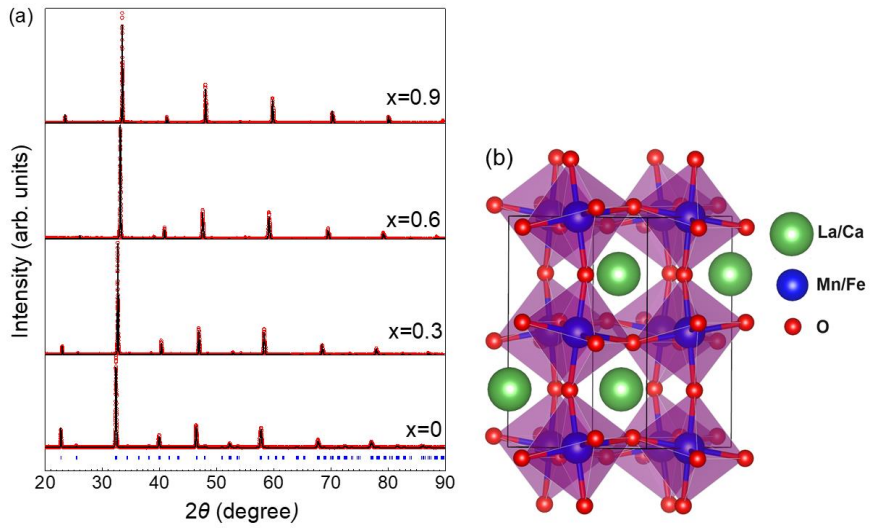

Figure 1. (a) XRD patterns at room temperature of the LCFMO samples: the experimental points (red), calculated lines (black) and the position of the nuclear peak (blue) are shown.
(b) Crystal structure of *Pnma* tetragonal phase LCFMO

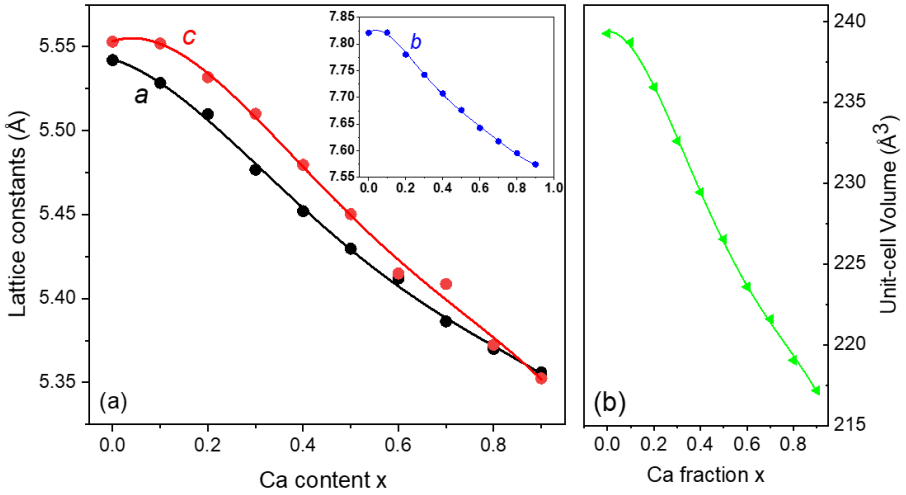

Figure 2. Effect of the Ca content *x* on (a) lattice parameters and
(b) unit-cell volume of LCFMO compounds

Furthermore, the crystallite size *D* and microstrain ε in the LCFMO samples were determined from the XRD data using the Williamson-Hall equation based on the dependence of the diffraction peak broadening β (after subtracting the instrumental contribution) on its 2θ position (Li *et al*., 2014):

$$\beta\cos\theta = \frac{K\lambda}{D} + 4\varepsilon\sin\theta\,, \qquad (1)$$

where, *K* is the Scherrer constant (0.9), λ is the wavelength of the X-ray (0.154056 nm), β is the FWHM of XRD peak due to microsize of crystal and θ is the Bragg angle.

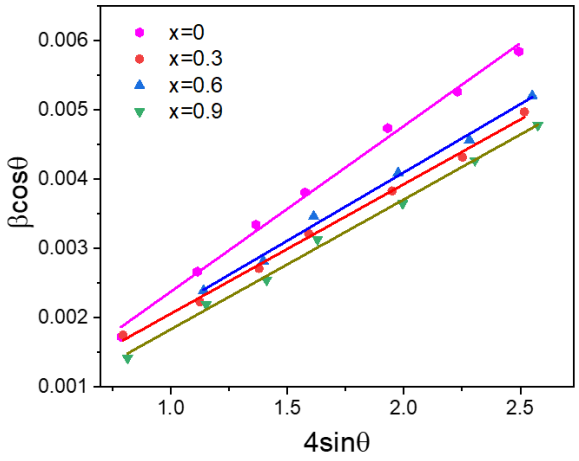

Figure 3. Dependence of βcosθ on 4sinθ of the LCFMO samples

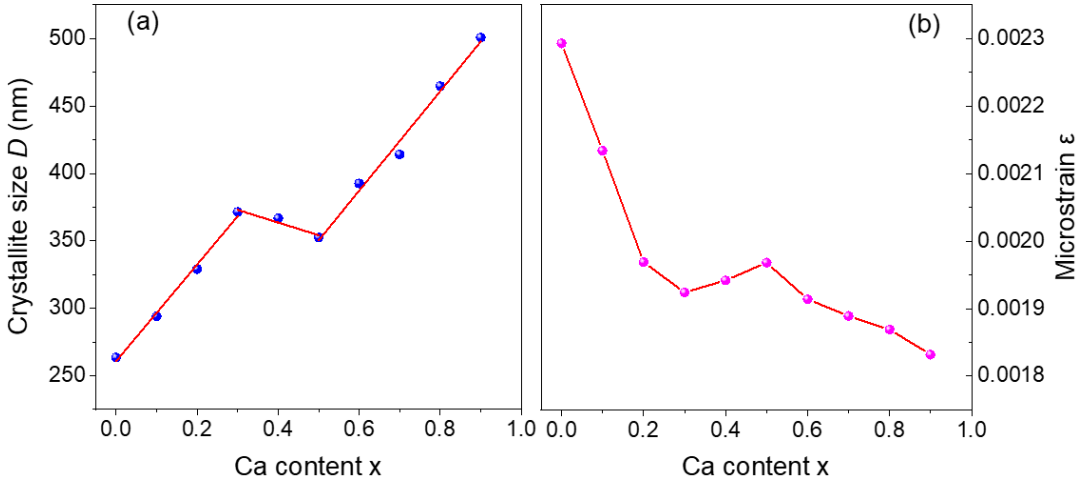

Figure 4. Ca-content dependence of (a) crystallite size and (b) microstrain of the LCFMO samples

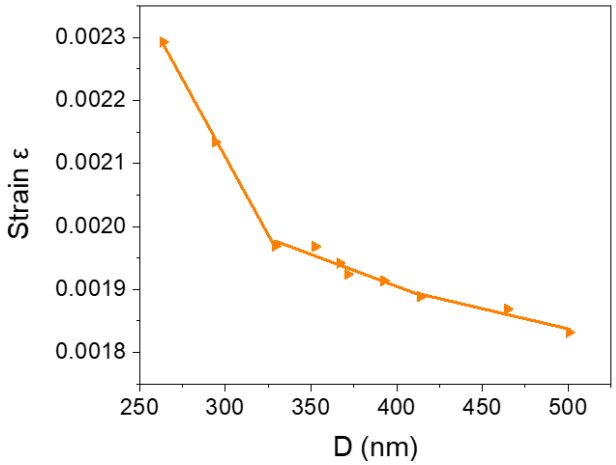

Figure 5. Dependence of the microstrain on the crystallite size of LCFMO samples

From Equation (1), by plotting the dependence of $\beta\cos\theta$ on $4\sin\theta$ (Figure 3), we can determine the crystallite size D and microstrain ε from the intersection point of the graph

βcosθ vs 4sinθ with the vertical axis β.cosθ and the slope of this graph, respectively. Figure 4 shows the dependence on the Ca-doping content of the crystallite size and microstrain of the LCFMO compounds. It can be seen that both parameters change anomalously. The crystallite size increases at x = 0.3, then decreases abnormally to x = 0.5 and continues to increase. Meanwhile, microstrain shows an opposite change trend with the crystallite size. The dependence of the microstrain on the crystallite size are also plotted. As shown in Figure 5, the microstrain increases as the crystallite size decreases. This is possibly due to the enhancement of structural defects with decreasing the crystallite size.

In addition, other structural parameters such as bond length and angle in BO_6 octahedra were also determined from the XRD refinement. Similar to the lattice constants, as the doping concentration increases, the average B-O bond length decreases, as shown in Figure 6(a). However, the average B-O-B bond angle increases with respect to the doping concentration, resulting in the increase in the tilt angle of octahedra as shown in Figure 7. The dependence on the doping concentration of lattice parameters of the samples are also present in Table 1.

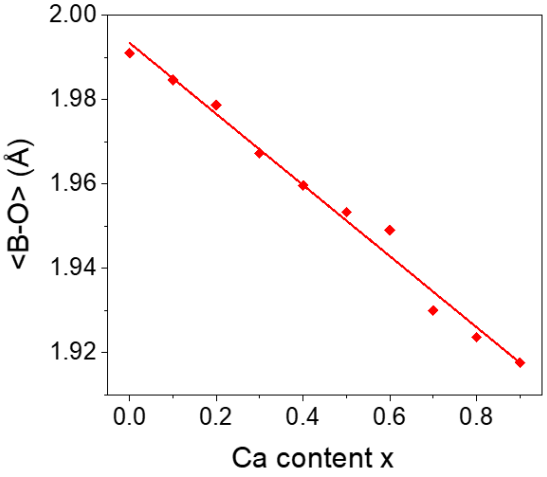

Figure 6. Ca-content dependence of the average B-O bond length in the LCFMO samples

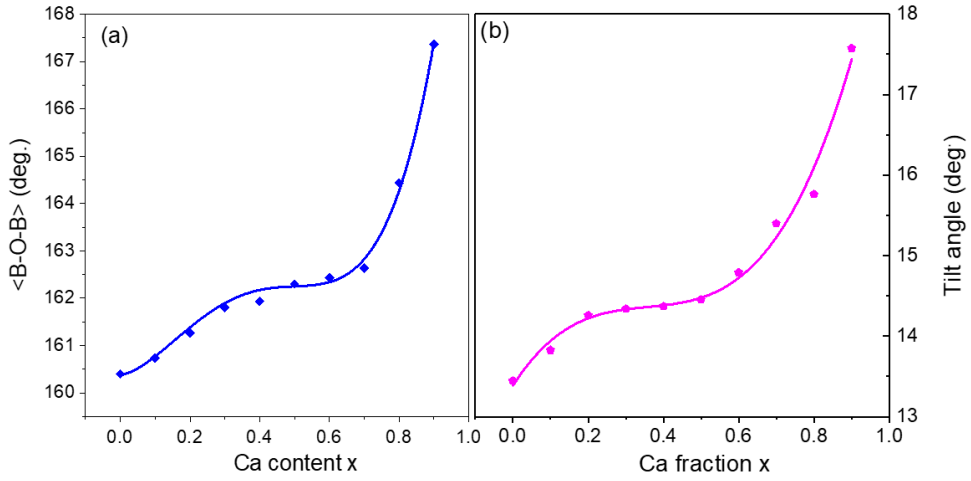

Figure 7. Ca-content dependence of (a) B-O-B bond angle average, (b) tilt of the octahedra of LCFMO

Table 1. Structural parameters such as bond lengths, bond angles, distortion parameter Δd of octahedron with an average B-O distance <d> ($\Delta d = (1/6)\sum_{n=1,6}[(d_n - \langle d\rangle)/\langle d\rangle]^2$ (Rodríguez-Carvajal *et al.*, 1998) and titl angle $\varphi = -\sqrt{48} \times tan^{-1}(y[O_2])$ (O'Keeffe & Hyde, 1977) of the LCFMO samples. Atom positions in *Pnma*: |R (La/Ca) 4*c* (x, 0.25, z); B (Mn/Fe) 4*b* (0, 0, 0.5); O1 4*c* (x, 0.25, *z*) and O2 8*d* (x, y, *z*)

x	0	0.1	0.2	0.3	0.4	0.5	0.6	0.7	0.8	0.9
B1-O1(1) (Å)	1.973	1.96	1.959	1.95	1.945	1.937	1.943	1.939	1.933	1.931
B1-O2(1) (Å)	2.025	2.015	2.01	1.998	1.987	1.982	1.975	1.945	1.937	1.926
B1-O2(2) (Å)	1.975	1.979	1.967	1.954	1.944	1.941	1.941	1.906	1.901	1.896
<B-O> (Å)	1.991	1.985	1.979	1.967	1.960	1.953	1.95	1.93	1.924	1.918
Δd (× 10^4)	1.459(7)	1.320(7)	1.281(1)	1.221(8)	1.198(4)	1.083(8)	0.636(2)	0.789(2)	0.701(4)	0.649(6)
B-O1-B (deg.)	168.6	170.4	168.6	166.2	165.4	164.1	163.3	161.5	158.7	157.3
B-O2-B (deg.)	156.3	155.9	157.6	159.6	160.2	161.3	162	163.3	167.3	172.4
<B-O-B> (deg.)	160.4	160.7	161.3	161.8	161.9	162.3	162.4	162.6	164.4	167.4
φ (deg.)	13.4(4)	13.8(2)	14.2(5)	14.3(3)	14.3(7)	14.4(5)	14.7(9)	15.3(8)	15.7(6)	17.5(7)

Raman spectroscopy is a highly sensitive spectroscopic technique for probing the local crystal structure and vibration modes strongly depending on the structural phase of materials, so Raman studies have been conducted to gain a better understanding of the phase structure of Ca doped LCFMO.

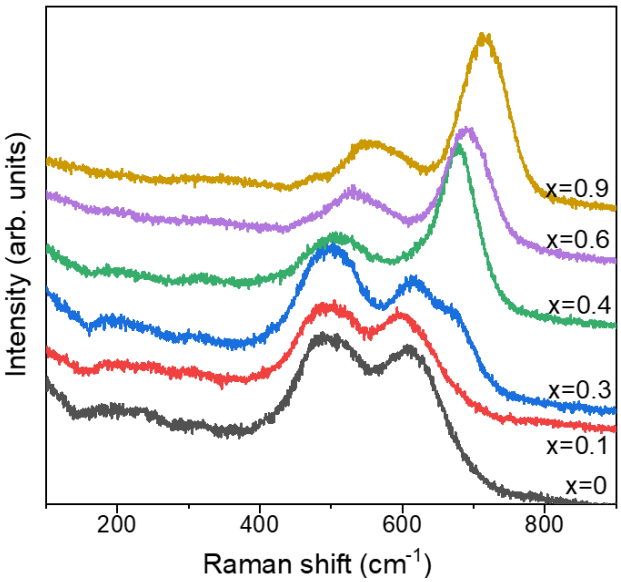

Figure 8. Raman spectra of LCFMO compounds

Figure 8 shows the Raman spectra of some representative LCFMO samples (x = 0, 0.1, 0.3, 0.4, 0.6 and 0.9). The Raman spectrum of the LCFMO sample with x = 0 contains main peaks at 314, 474 and 605 cm^{-1}, which are characteristic Raman modes of LCFMO

(Bhame *et al*., 2005; Dhilip *et al*., 2019; Nasir *et al*., 2020; Palakkal *et al*., 2018; Triyono *et al*., 2021; Wu *et al*., 1994). Peaks at 314 and 474 cm^{-1} are associated with the bending of the Fe/MnO_6 octahedral cluster with the A_g symmetry, while peak at 605 cm^{-1} corresponds to the stretching of the Fe/MnO_6 octahedral cluster with the B_{1g} symmetry, which is attributed to the strong spin-lattice interaction (Iliev & Abrashev, 1998; Nasir *et al*., 2020; Triyono *et al*., 2021). In addition, the Raman intensity of the samples is enhanced as increasing the Ca-doping content *x*, indicating a reduced crystal lattice distortion. This result is consistent with the observed orthorhombic lattice distortion revealed by the XRD analysis (Table 1).

In addition, the Raman spectra in Figure 8 also show a significant frequency shift towards the larger frequency of the mode B_{1g} at ~ 605 cm^{-1} and a broadening of peak at 474 cm^{-1} as increasing the dopant concentration. This demonstrates a suppression of Jahn–Teller (JT) distortion of Fe/MnO_6 octahedra in the LCFMO samples with respect to the doping concentration. The suppression of JT distortion is possible related to an increase of Mn^{4+} ions in the Ca-doped samples for reasons of valence conservation as increasing the substitution of Ca^{2+} for La^{3+} (Baldini *et al*., 2009). Furthermore, the Raman spectra in Figure 8 also show a change in the relative intensity of peaks at 474 and 605 cm^{-1} with respect to *x*. It can be seen that the relative intensity of the peak at 474 cm^{-1} decreases, while that of the peak at 605 cm^{-1} increases as the Ca doping content increases. These results demonstrate that the presence of Ca^{2+} ions affect the bending and stretching of the Fe/MnO_6 octahedra.

4. Conclusions

Perovskite materials of $La_{1-x}Ca_xFe_{0.5}Mn_{0.5}O_3$ (x = 0, 0.1, 0.2, 0.3, 0.4, 0.5, 0.6, 0.7, 0.8 and 0.9) were synthesized utilizing the conventional ceramic method. The influence of the Ca-doping on the structural properties of the compounds were studied using the measurements of X-ray diffraction and Raman scattering spectroscopy. The Rietveld refinement analysis of XRD data shows that all the samples are single phase with the orthorhombic crystal structure belonging to the space group of *Pbnm*. The results demonstrate the influence of doping on structural parameters such as lattice parameters, crystallite size, microstrain, bond length and angle in the samples.

Acknowledgments

This research was supported by Project Grant No: T2023-69, funded by Ho Chi Minh City University of Technology and Education (Vietnam).

References

Ahmad, J., Yasmin, M., Ahmad, U., Bukhari, S.H., Nissar, U., Khan, J.A. & Abbas, H. (2021). Structural, optical and electrical properties of alkaline earth doped $La_{2-x}A_xFeMnO_6$ (A = Ca, Sr and Ba) double perovskites. *Journal of Nanoscope (Jn)*, *2*(1), 69–91.

Baldini, M., Di Castro, D., Cestelli-Guidi, M., Garcia, J. & Postorino, P. (2009). Phase-separated states in high-pressure $LaMn_{1-x}Ga_xO_3$ manganites. *Physical Review B*, 80, 045123.

Bhame, S.D., Joly, V.L.J. & Joy, P.A. (2005). Effect of disorder on the magnetic properties of $LaMn_{0.5}Fe_{0.5}O_3$. *Physical Review B - Condensed Matter and Materials Physics*, *72*(5), 054426.

Dagotto, E., Burgy, J. & Moreo, A. (2003). Nanoscale phase separation in colossal magnetoresistance materials: Lessons for the cuprates? *Solid State Communications*,

126(1–2), 9–22.

Dar, S.A., Murtaza, G., Zelai, T., Nazir, G., Alkhaldi, H., Albalawi, H., Kattan, N.A., Irfan, M., Mahmood, Q. & Mahmoud, Z. (2023). Study of structural, electronic, magnetic and optical properties of A_2FeMnO_6 (A = Ba, La) double perovskites, experimental and DFT analysis. *Colloids and Surfaces A: Physicochemical and Engineering Aspects*, 664, 131145.

Das, S., Mali, B., Ganesan, R. & Elizabeth, S. (2023). Observation of griffiths phase and ferromagnetism in $LaFe_{0.5}Mn_{0.5}O_3$. *Materials Research Bulletin*, 160, 112128.

De Lima, O.F., Coaquira, J.A.H., De Almeida, R.L. & Malik, S.K. (2010). Magnetic phase separation and cluster-spin-glass behavior in $LaMn_{1-x}Fe_xO_{3+y}$. *Journal of Applied Physics*, *107*(9), 09E107.

De, K., Ray, R., Narayan Panda, R., Giri, S., Nakamura, H. & Kohara, T. (2005). The effect of Fe substitution on magnetic and transport properties of $LaMnO_3$. *Journal of Magnetism and Magnetic Materials*, 288, 339–346.

De, K., Thakur, M., Manna, A. & Giri, S. (2006). Unusual glassy states in $LaMn_{0.5}Fe_{0.5}O_3$: Evidence of two distinct dynamical freezing processes. *Journal of Applied Physics*, *99*(1), 013908.

Dhilip, M., Devi, N.A., Punitha, J.S., Anbarasu, V. & Kumar, K.S. (2019). Conventional synthesis and characterization of cubically ordered La_2FeMnO_6 double perovskite compound. *Vacuum*, 167, 16–20.

Dutta, U., Hossain, A., Walke, P.S., Ghosh, D., Mordvinova, N.E., Lebedev, O.I., Haque, A., Pal, K., Gayen, A., Kundu, A.K. & Seikh, M.M. (2019). Synthesis, structure and magnetic properties of nanodimensional $La_{1-x}BaxFe_{0.5}Mn_{0.5}O_3$ perovskites. *Journal of Alloys and Compounds*, 777, 1396–1402.

Geng, X., Xie, Y., Ma, Y., Liu, Y., Luo, J., Wang, J., Yu, R., Deng, B. & Zhou, W. (2020). Abnormal thermal quenching and application for w-LEDs: Double perovskite $Ca_2InSbO_6:Eu^{3+}$ red-emitting phosphor. *Journal of Alloys and Compounds*, 847, 156249.

Gerra, G., Tagantsev, A.K., Setter, N. & Parlinski, K. (2006). Ionic polarizability of conductive metal oxides and critical thickness for ferroelectricity in $BaTiO_3$. *Physical Review Letters*, *96*(10), 107603.

Gilleo, M.A. (1957). Crystallographic studies of perovskite-like compounds. III. $(Mn_{1-x})O_3$ with M = Co, Fe and Cr. *Acta Crystallographica*, *10*(3), 161–166.

Glazer, A.M. (1972). The classification of tilted octahedra in perovskites. *Acta Crystallographica Section B Structural Crystallography and Crystal Chemistry*, *28*(11), 3384–3392.

Granado, E., Moreno, N., García, A., Sanjurjo, J., Rettori, C., Torriani, I. & Oseroff, S. (1998). Phonon Raman scattering. *Physical Review B - Condensed Matter and Materials Physics*, *58*(17), 11435–11440.

Guo, W., Liu, X., Han, S., Liu, Y., Xu, Z., Hong, M., Luo, J. & Sun, Z. (2020). Room-temperature ferroelectric material composed of a two-dimensional metal halide double perovskite for X-ray detection. *Angewandte Chemie - International Edition*, *59*(33), 13879–13884.

Hossain, A., Ghosh, D., Dutta, U., Walke, P.S., Mordvinova, N.E., Lebedev, O.I., Sinha, B., Pal, K., Gayen, A., Kundu, A.K. & Seikh, M.M. (2017). Synthesis, structure and magnetic properties of nanostructured $La_{1-x}A_xFe_{0.5}Mn_{0.5}O_3$ (A = Ca, Sr and Pb; x = 0 & 0.25) perovskites. *Journal of Magnetism and Magnetic Materials*, 444, 68–76.

Iliev, M., Abrashev, M. (1998). Raman spectroscopy of orthorhombic perovskitelike $YMnO_3$ and $LaMnO_3$. *Physical Review B - Condensed Matter and Materials Physics*, *57*(5), 2872–2877.

Jafarov, M. A., Nasirov, E. F., Kazımzade, A. H., & Jahangirova, S. A. (2021). Synthesis and characterization of nanoscale material ZnS in porous silicon by chemical method. *Chalcogenide Lett*, *18*(12), 791-795.

Li, Q.H., Li, N., Hu, J.Z., Han, Q., Ma, Q.S., Ge, L., Xiao, B. & Xu, M.X. (2014). The effect of Ca-substitution in La-site on the magnetic properties of La_2CoMnO_6. *Journal of Applied Physics*, *116*(3), 033905.

Lu, Z., Meng, Y., Wen, L., Huang, M., Zhou, L., Liao, L. & He, D. (2019). Double perovskite $Ba_2LaNbO_6:Mn^{4+},Yb^{3+}$ phosphors: Potential application to plant-cultivation LEDs. *Dyes*

and Pigments, 160, 395–402.

MącZka, M., Ptak, M., Luz-Lima, C., Freire, P.T.C., Paraguassu, W., Guerini, S. & Hanuza, J. (2011). Pressure-induced phase transitions in multiferroic $RbFe(MoO_4)_2$ - Raman scattering study. *Journal of Solid State Chemistry*, *184*(10), 2812–2817.

Martínez-Rodríguez, H.A., Jurado, J.F. & Restrepo-Parra, E. (2018). Electrical conductivity behavior of $La_{0.5}Ca_{0.5}Mn_{0.5}Fe_{0.5}O_3$ synthetized by the solid state reaction. *Modern Applied Science*, *12*(12), 174.

Mitchell, R.H. (2002). *Perovskites: Modern and Ancient*, part of chapter 8, 181–194. Canada.

Nasir, M., Khan, M., Agbo, S.A., Bhatt, S., Kumar, S. & Sen, S. (2020). Evidence of cluster-glass and Griffiths-like phases in partially ordered La_2FeMnO_6 double perovskite. *Journal of Physics D: Applied Physics*, *53*(37), 325–333.

O'Keeffe, M., Hyde, B.G. (1977). Some structures topologically related to cubic perovskite (E21), ReO_3(D09) and Cu_3Au(L12). *Acta Crystallographica B*, 33, 3802–3813.

Palakkal, J.P., Sankar, C.R., Paulose, A.P. & Varma, M.R. (2018). Hopping conduction and spin glass behavior of La_2FeMnO_6. *Journal of Alloys and Compounds*, 743, 403–409.

Pantoja, A.E., Trodahl, H.J., Buckley, R.G., Tomioka, Y. & Tokura, Y. (2001). Raman spectroscopy of orthorhombic $La_{1-x}Ca_xMnO_3$, x = 0.1-0.3. *Journal of Physics Condensed Matter*, *13*(16), 3741–3752.

Rini, E.G., Gupta, M.K., Mittal, R., Mekki, A., Al Saeed, M.H. & Sen, S. (2021). Structural change from Pbnm to $R\bar{3}c$ phase with varying Fe/Mn content in $(1-x)LaFeO_3.xLaMnO_3$ solid solution leading to modifications in octahedral tilt and valence states. *Journal of Alloys and Compounds*, 883, 160761.

Rodríguez-Carvajal, J., Hennion, M., Moussa, F., Moudden, A., Pinsard, L. & Revcolevschi, A. (1998). Neutron-diffraction study of the Jahn-Teller transition in stoichiometric. *Physical Review B - Condensed Matter and Materials Physics*, *57*(6), R3189–R3192.

Romero, M., Faccio, R., Martínez, J., Pardo, H., Montenegro, B., Plá Cid, C.C., Pasa, A.A. & Mombrú, Á.W. (2015). Effect of lanthanide on the microstructure and structure of $LnMn_{0.5}Fe_{0.5}O_3$ nanoparticles with Ln=La, Pr, Nd, Sm and Gd prepared by the polymer precursor method. *Journal of Solid State Chemistry*, 221, 325–333.

Triyono, D., Yunida, Y. & Rafsanjani, R.A. (2021). Effect of heat treatment on structural, magnetic and electrical properties of La_2FeMnO_6. *Materials*, *14*(24), 7501.

Woodward, P.M. (1997). Octahedral Tilting in Perovskites. I. Geometrical Considerations. *Acta Crystallographica Section B: Structural Science*, *53*(1), 32–43.

Wu, Y., Yu, Z. & Liu, S. (1994). Preparation, crystal structure and vibrational spectra of perovskite-type mixed oxides $LaM_yM'_{1-y}O_3$ (M, M′ = Mn, Fe, Co). *Journal of Solid State Chemistry*, *112*(1), 157–160.

Zhang, W., Hong, M. & Luo, J. (2020). Halide double perovskite ferroelectrics. *Angewandte Chemie - International Edition*, *59*(24), 9305–9308.